International Journal of Refrigeration 137 (2022) 22–33

Contents lists available at ScienceDirect

International Journal of Refrigeration

journal homepage: www.elsevier.com/locate/ijrefrig

Energy impact of the Internal Heat Exchanger in a horizontal freezing cabinet. Experimental evaluation with the R404A low-GWP alternatives R454C, R455A, R468A, R290 and R1270

Impact énergétique de l'échangeur de chaleur interne dans une armoire de congélation horizontale. Évaluation expérimentale des alternatives à faible PRP au R404A : R454C, R455A, R468A, R290 et R1270

Ramón Cabello *, Daniel Sánchez, Rodrigo Llopis, Alejandro Andreu-Nacher, Daniel Calleja-Anta

Jaume I University, Dep. of Mechanical Engineering and Construction, Campus de Riu Sec s/n, E-12071, Castellón, Spain

ARTICLE INFO

KEYWORDS:
R404a
R290
R1270
R454c
R455A
R468A

Mots clés:
R290
R1270
R454C
R455A
R468A
R404A

ABSTRACT

This work analyses the influence of the Internal Heat Exchan ger (IHX) on the energy performance of a vapor compression cycle associated with a freezing cabinet using different R404A low-GWP alternatives. Among them, the refrigerants R454C (GPW_{100}=146), R455A (GPW_{100}=146), R468A (GPW_{100}=146), R290 (GPW_{100}=5) and R1270 (GPW_{100}=1.8) have been tested in a horizontal freezing cabinet maintaining a product target temperature of -20°C at the heat rejection temperatures of 20, 30 and 40°C. The results from tests show that the use of the IHX reduces energy consumption in all scenarios without significantly increasing the compressor's discharge temperature. For a test period of 16 h, the refrigerants that offer better reductions are R404A and R1270, followed by R455A, R290, R454C and R468A. The maximum energy saving is rated to 9.2% at the heat rejection temperature of 40°C, demonstrating that the enhancement of the IHX is better as higher the heat rejection conditions are.

1. Introduction

Refrigeration facilities contributes to the global warming in a direct way (through refrigerants leaks, especially with those which have high global warming potential) and in an indirect way (through the energy consumption, since this energy it is generated with a technology mix that releases CO_2 to the environment) (AIRAH 2012; Makhnatch and Khodabandeh, 2014). These two ways represented, respectively the 37% and 63% of direct and indirect CO_2 equivalent emissions in the refrigeration field in 2018, what represented the 7.8% of global GHG emissions, as is stated in (Lebrun and Ziegler, 2019)

Once the direct effect it is being smoothed via the utilization of low-GWP refrigerants, the research in the refrigeration field is being focused on the improving of the energy efficiency of its facilities. This is in tune with international regulations, like the Energy Efficiency Directive 2018/2002 in Europe that proposes a reduction for 2030 of 32.5% of the primary energy demand based on 2007 demand (Directive (EU) 2018).

The incorporation of a heat exchanger that transfers heat internally in the mechanical vapor compression cycle, from liquid to suction line, is a technique used mainly at its beginning to produce a useful superheat at the suction line. The usefulness comes from the fact that the superheating in the evaporator can be minimized, because the IHX ensures that no liquid enters the compressor, while gets an additional subcooling at expansion valve inlet, increasing, thus, the evaporator cooling capacity (Gosney, 1982; Emerson Climate Technologies 1993).

The IHX influence on the energy performance of the cycle was studied later, at 90 s. Authors like Domanski, (Domanski et al., 1994;

* Corresponding author.
E-mail address: cabello@uji.es (R. Cabello).

https://doi.org/10.1016/j.ijrefrig.2022.02.007
Received 27 October 2021; Received in revised form 17 January 2022; Accepted 8 February 2022
Available online 10 February 2022

NOMENCLATURE

COP	coefficient of performance
E	energy consumption (kW•h)
EEV	Electronic Expansion Valve
GHG	Green House gasses
GWP_{100}	Global warming potential, 100 years horizon
h	specific enthalpy ($kJ•kg^{-1}$)
IHX	Internal Heat Exchanger
$\dot{m}$	mass flow rate ($kg•s^{-1}$)
NBP	Normal Boiling Point (°C)
ODP	Ozone Depleting Potential
p	pressure (kPa)
P_C	power consumption (kW)
$\dot{Q}_O$	cooling capacity (kW)
q_o	specific cooling capacity ($kJ•kg^{-1}$)
RH	Relative Humidity (%)
r_p	compressor pressure ratio
SH	superheating (K)
SC	subcooling (K)
T	temperature, (K or °C)
t	time (s)
u	uncertainty (%)
v	specific volume ($m^3•kg^{-1}$)
VCC	Volumetric Cooling Capacity ($kJ•m^{-3}$)
x_v	vapor quality

GREEK SYMBOLS

λ	latent heat of phase-change ($kJ•kg^{-1}$)
Δ	Prefix, means preceding variable variation
η_v	volumetric efficiency

SUBSCRIPTS

air	air return to evaporator
c	critical point
dis	compressor discharge
in	inlet
k	condensing level
o	evaporating level
out	outlet
sat,l	saturated liquid
sat,v	saturated vapor
suct	compressor suction

Domanski, 1995), Aprea (Aprea et al., 1999) or Klein (Klein et al., 2000), tried to stablish a theoretical criterion that showed the increment or decrement in COP due to the IHX. Those criteria were based on thermodynamic analysis of the cycle and thermophysical properties of the working fluids. They were useful to detect the main factors that influenced the energy performance: the refrigerant, the pressure drops at the IXH and the IHX efficiency, among others.

At the first years of 21st century experimental studies like those of Ahnefeld et al. (Ahnefeld et al., 1996), Boewe et al. (Boewe et al., 2001), Kim (Kim, 2002), Zhang et al. (Zhang et al., 2002) or Navarro-Esbrí et al. (Navarro-Esbri et al., 2005) were published. They certified the results obtained at theoretical studies and the upgrade in the energy efficiency achieved with the IHX in many cases.

Recently for the second decade of 21st century many works both experimental and theoretical, dealing with internal heat exchanger effect on the mechanical vapor compression cycle have been published. Those publications could be mainly classified into the ones that study the effect of the IHX on refrigeration and heat pump facilities working with CO_2, and the ones analyzing the effect on refrigeration facilities working with R134a and its substitutes. Among the first ones can be highlighted Torrella et al. (Torrella et al., 2022), Sanchez et al. (Sánchez et al., 2014), Purohit et al. (Purohit et al., 2018), Cao et al. (Cao et al., 2020) and Ye et al. (Ye et al., 2020), they demonstrates experimentally that IHX is beneficial for this kind of refrigeration facilities working in medium/high evaporating temperature range increasing their cooling capacity and COP, however, Zhang et al. (Zhang et al., 2013) and Joneydi et al. (Joneydi Shariatzadeh et al., 2016), obtain from theoretical models that combine IHX with vapor compression cycles using ejectors or expanders, respectively, do not produce improvements in the cycle performance. Among the second ones Cabello et al. (Cabello et al., 2015), Navarro-Esbrí et al. (Navarro-Esbrí and Molés, 2013), Qi (Qi, 2015), Mota et al. (Mota-Babiloni et al., 2019) and Wantha (Wantha, 2019), obtain from experimental data and theoretical models that IHX improves slightly COP and cooling capacity of vapor compression plants working with R134a or R152a, but further improvements are found if working with R1234y or R513A. If the above works are related to single stage vapor compression cycle, other works like those of Cabello et al. (Cabello et al., 2017) and Llopis et al. (Llopis et al., 2015,2016) studied the effect of the IHX in low temperature cycle of cascade refrigeration plants, showing the benefic effect of the IHX on the energy efficiency of the cascade refrigeration plant.

Therefore, in the current picture, where new low and ultra-low GWP refrigerant fluids (simple or blends) are brought to market to replace R404A in low temperature applications used in commercial refrigeration, it is interesting to know if the utilization of IHX in freezing cabinets with those refrigerant, is a useful energy saving measure. The present work provides experimental data obtained from a real refrigeration facility with a low temperature (LT) service, performed by chest freezing cabinet with door glasses, working with the new low GWP blends based on HFO: R454C, R455C and R468A, and with the ultra-low GWP natural fluids: R290 (propane) and R1270 (propylene). Tests have been done to cover a wide range of environmental conditions, so it has been selected three heat rejection conditions: 20°C, 30°C and 40°C. The heat source has been set to a temperature level of −20°C in all tests, in such way that the compressor is continuously running and stopping in accordance with the freezing cabinet regulation, what leads to a non-steady state tests.

As the aim of the work is to analyze the IHX influence on the energy performance, for comparison purposes, all tests have been repeated in the same heat source and heat sink conditions with and without the IHX activation.

A dropping methodology on a scaled commercial refrigeration plant has been applied to get a comparison nearest to the actual energy behavior. Only the compressor has been changed when hydrocarbons are used, and adjustments in the parameters at the electronic expansion valve has been done to its proper operation.

2. Thermodynamic properties and theoretical performance

2.1. Refrigerants thermophysical properties comparison

In this work we use six refrigerants, R404A, which is the working fluid serving as the basis of comparison, and five low and ultra-low GWP refrigerant alternatives at low evaporating temperatures, three HFC/HFO blends: R454A, R455A and R468A, and two hydrocarbons: R290, R1270. The main properties of those refrigerants are listed in Table 1.

Among them, R468A, R454C and R455A are non-azeotropic blends based mainly in the HFC R32 and the HFO R1234yf, both with an anthropogenic origin. They are included into the low-GWP fluorinated refrigerants category while R290 and R1270 are single and natural refrigerants, with ultra low GWP following the classification proposed by

Table 1
Refrigerants main properties.

Refrigerant	R404A	R468A	R454C	R455A	R290	R1270
Components[1]	HFC125 / HFC143a / HFC134a	HFC32 / HFO1234yf / HFO1132a	HFC32 / HFO1234yf	R744 / HFC32 / HFO1234yf	Propane	Propylene
Composition (%weight) [1]	44 / 52 / 4	21.5 / 75 / 3.5	21.5/78.5	3.0/21.5/75.5	100	100
ODP[1]	0	0	0	0	0	0
GWP_{100} (AR5)[2]	3943	146	146	146	5	1.8
Safety Class [1]	A1	A2L	A2L	A2L	A3	A3
Molecular Weight ($kg \bullet kmol^{-1}$)[1]	97.6	88.84	90.8	87.5	44.1	42.1
T_c (K / °C) [1]	345.27 / 72.12	362.31 / 89.16	358.82 / 85.67	358.76 / 85.61	369.89 / 96.74	364.21 / 91.06
P_c (kPa) [1]	3750	4378	4318.77	4653.8	4251.2	4550
ρ_c ($kg \bullet m^{-3}$)[1]	486.70	444.27	461.59	454.89	220.48	229.63
NBP (K) (liq. / vap.)	226.65 / 227.41-	210.02 / 236.82	227.31 / 235.12	220.85 / 233.7	230.74	225.24
$Glide_o$ *,[3]	0.657	24.5	7.86	12.64	0	0
$Glide_k$ **,[3]	0.336	12.6	6.81	9.84	0	0
$v_{sat.v}$ ($m^3 \bullet kg^{-1}$)*,[3]	0.0932	0.1457	0.1235	0.11498	0.2586	0.25878
$v_{sat.liq}$ ($m^3 \bullet kg^{-1}$)*,[3]	0.000780	0.000796	0.000805	0.000801	0.001765	0.001682
λ_o ($kJ \bullet kg^{-1}$)*,[3]	190	246	219.475	229.43	412.41	424.696
λ_k ($kJ \bullet kg^{-1}$)**,[3]	120	171	153.74	159.51	307.07	306.79
VCC ($kJ \bullet m^{-3}$)*,[3]	2039	1688	1777	1995	1595	1641

[1] ASHRAE (ASHRAE 2019)
[2] IPCC (Zhang, 2014)
[3] Refprop v.10 (Lemmon et al., 2018).
* Calculated for a pressure corresponding to a temperature of 243 K (−30 °C) and x_v=0.5.
** Calculated for a pressure corresponding to a temperature of 313 K (40 °C) and x_v=0.5 (.

UNEP (UNEP 2019). Due to those GWP values none of those refrigerants are penalized with the taxes that some countries have applied to greenhouse gasses. The safety classification of anthropogenic refrigerants is A2L, and of hydrocarbons is A3, given by ASHRAE (ASHRAE 2019). This flammable character balances their environmental advantages, what is the common characteristics of most refrigerants currently available apart from R744. This is why they are subject to safety regulations that affect to refrigeration equipment, like EN378, EN60335, ISO 5149 and IEC 60,335. These regulations are revising their standards to increase the flammable refrigerant charge size limits what will allow a higher charge, making possible A2L and A3 refrigerants to be used in a wider range of applications.

If we compare the molecular weight of the alternative refrigerants tested to that of R404A, they are “lighter”, around 5.5% to 10% in case of anthropogenic ones, and 55% to 57% in case natural ones. This is preferable to reduce the compressor energy losses across valves (Woollatt., 1993) and to get higher vaporization enthalpies. The critical temperature and pressure of R468A, R454C, R455A,R290 and R1270 are greater than those of R404A, what supposes that the vapor compression cycle will operate at lower reduced temperatures and pressures, generally resulting in higher efficiencies but lower volumetric cooling capacity (VCC), and also the requirement of a physically larger equipment, specially the compressor displacement or its running time, depending on the type of regulation (McLinden et al., 2012).

The NBP of all refrigerants used in this work is low enough to assure the operation of the cycle above the atmospheric pressure, avoiding the possibility of air intake in the sealed circuit with the subsequent performance degradation of the lubricant oil and heat exchangers, as well as the generation of an internal loop explosion hazard in case of flammable refrigerants.

Glide values at Table 1, show that alternative anthropogenic refrigerants present much greater values in comparison with R404A ones in the whole saturation range, especially R468A. So, in those refrigerants if a proper glide matching is designed, the higher glide value could be an advantage to improve the heat transfer in the evaporator and condenser, and could result in a better cycle energy performance [(Torrella et al., 2010; Marques and Domanski, 1998)and (M et al., 2017)]. Conversely, the natural refrigerants do not present glide because they are single refrigerants. Only the pressure losses at heat exchangers could generate a temperature difference during the evaporation and condensation. The different vapor saturation curves make necessary to reprogram the electronic expansion valves, programming fine new interpolation polynomials for each fluid to get proper regulation.

2.2. Theoretical performance of the IHX

A simple vapor compression cycle has been considered to simulate the influence of the IHX at the energy behavior. The evaporating temperature has been selected to represent the low temperature application conditions, as well as a wide range in heat sink temperatures to cover the different environmental conditions at condenser.

Those specifications are: evaporating temperature of −35°C / 238 K; condensing temperatures of 40°C / 313 K and 20°C / 293 K, no evaporator superheat nor condenser subcooling are set, pressure drop at refrigerant lines and heat exchangers have been disregarded as well as the heat losses/gains to/from the ambient; the compressor isentropic efficiency is assumed to be 100% and the internal heat exchanger thermal efficiencies of 0% (no IHX) and 50%. To compare the mass flow rate driven by the compressor and its power consumption, a cooling capacity of 1000 W has been used as a reference.

To consider the high glide of R468A, R454C and R455A, the phase change pressures has been calculated from the corresponding saturation temperatures, using the criteria recommended by ASERCOM ASERCOM 2015). This way, the condensing pressure has been evaluated for a vapor title of 50% at the given T_k as presented in Eq. (1), and the evaporating pressure using the average enthalpy value at the evaporator, Eq. (2). The rest of variables used at this section, like the refrigerant mass flow rate, the specific cooling capacity, the volumetric cooling capacity, the compressor work rate, the coefficient of performance and the IHX thermal effectiveness are calculated using Eqs. (3) to ((8), respectively, according to scheme shown in Fig. 1. The results are gathered at Table 2. All the thermodynamic properties were evaluated using Refprop v10.0 (Lemmon et al., 2018).

$$p_k = f(T_k,\ x_v = 0.5) \tag{1}$$

$$p_o = f\left(T_o, \frac{h_{o,in} + h_{sat.v}(p_o)}{2}\right) \tag{2}$$

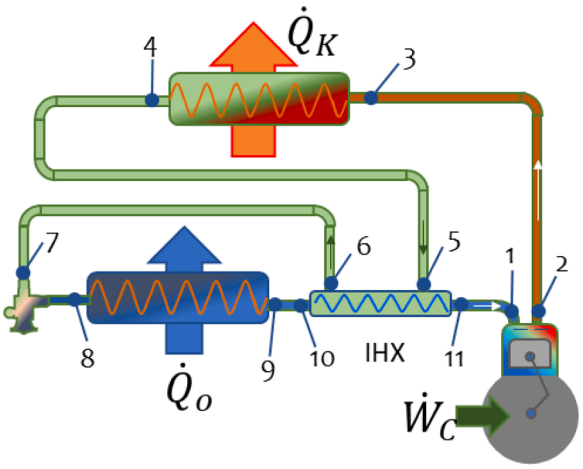

Fig. 1. vapor compression cycle scheme, with IHX.

$$q_o = h_{o,out} - h_{o,in} \tag{3}$$

$$\dot{m}_r = \frac{\dot{Q}_o}{q_o} \tag{4}$$

$$\dot{W}_C = \dot{m}_r \cdot (h_2 - h_1) \tag{5}$$

$$VCC = \frac{q_o}{v_1} \tag{6}$$

$$COP = \frac{q_o}{h_2 - h_1} \tag{7}$$

$$\varepsilon_{IHX} = \frac{T_{11} - T_{10}}{T_5 - T_{10}} \tag{8}$$

From the theoretical data shown in table 2, it is inferred that the IHX improves the energy efficiency of the cycle regardless the working fluid used and the heat sink temperature, although the higher the temperature is, the higher the improvement is. So, the increase in energy efficiency ranges from 3.65% with R1270 to 11% with R404A at 40°C heat sink temperature, what is due to, similar reductions in compressor electrical consumption. The IHX also produces a compressor discharge temperature increase, around 9%, higher for high heat sink temperatures. The volumetric cooling capacity (VCC) is other parameter affected by the activation of the IHX. It increases in all cases, since the specific cooling capacity augments in a greater magnitude than the suction specific volume does.

R404A is the refrigerant with better theoretical results with the IHX, while R1270 is the least influenced by the IHX. The rest of refrigerants presents values in a narrow range.

3. Experimental set-up description and test methodology

The experimental facility used in this work, as well as the methodology applied at the test campaign is similar to that described by Cabello eta al (Cabello et al., 2021). Following we explain the main characteristics needed to follow this paper.

Table 2
Energy parameters obtained in theoretical vapor compression cycle (T_o: −35°C; $\eta_{is.c}$: 1; ΔP: 0 kPa; SH: 0°C; SC: 0°C; $\dot{Q}_\varnothing$ = 1000 W).

			P_o	P_k	r_p	$\dot{m}_{ref}$	q_o	VCC	W_c	$x_{v,i}$	T_{dis}	COP
		IHX	(kPa)	(kPa)	–	($g \bullet s^{-1}$)	($kJ \bullet kg^{-1}$)	($kJ \bullet m^{-3}$)	(W)	–	(K)	–
R404A	T_k: 40 °C	ε_{IHX}: 0%	165.2	1823.1	11.04	11.5	86.7	754.5	558.2	0.554	323.9	1.79
		ε_{IHX}: 50%	165.5	1823.1	11.02	8.4	118.8	865.8	495.2	0.388	359.7	2.02
		% Variation				−36.90	27.02	12.86	−12.7	−42.78	9.95	11.4
	T_k: 20 °C	ε_{IHX}: 0%	165.5	1092.0	6.60	8.5	118.2	1030.1	321	0.391	302	3.12
		ε_{IHX}: 50%	165.7	1092.0	6.59	7.1	141.3	1078.1	309.2	0.272	328.9	3.23
		% Variation				−19.72	16.35	4.45	−3.82	−43.75	8.18	3.41
R468A	T_k: 40 °C	ε_{IHX}: 0%	114.9	1478.6	12.87	7.7	130	697.9	464.8	0.403	332.6	2.15
		ε_{IHX}: 50%	118.6	1478.6	12.47	6.3	157.7	754.1	439.9	0.288	364.5	2.27
		% Variation				−22.22	17.56	7.45	−5.66	−39.93	8.75	5.29
	T_k: 20 °C	ε_{IHX}: 0%	119.8	867.4	7.24	6.1	164.3	917.5	281.1	0.261	309.7	3.56
		ε_{IHX}: 50%	123.6	867.4	7.02	5.5	181.6	950.8	275.4	0.194	329.7	3.63
		% Variation				−10.91	9.53	3.50	−2.07	−34.54	6.07	1.93
R455A	T_k: 40 °C	ε_{IHX}: 0%	139.1	1741.6	12.52	8.3	121	773.9	501	0.424	335.1	2
		ε_{IHX}: 50%	144.0	1741.6	12.09	6.7	150.1	851.9	466.6	0.303	368.3	2.14
		% Variation				−23.88	19.39	9.16	−7.37	−39.93	9.01	6.54
	T_k: 20 °C	ε_{IHX}: 0%	144.6	1039.9	7.19	6.5	153.9	1020.7	303.7	0.288	312.2	3.29
		ε_{IHX}: 50%	148.1	1039.9	7.02	5.8	173.3	1058.1	296.6	0.211	334.9	3.37
		% Variation				−12.07	11.19	3.53	−2.39	−36.49	6.78	2.37
R454C	T_k: 40 °C	ε_{IHX}: 0%	126.6	1592.8	12.58	8.7	114.5	693.2	506.4	0.444	331.4	1.97
		ε_{IHX}: 50%	130.1	1592.8	12.24	6.9	144.7	767.2	467.9	0.312	366	2.14
		% Variation				−26.09	20.87	9.65	−8.23	−42.31	9.45	7.94
	T_k: 20 °C	ε_{IHX}: 0%	130.3	945.8	7.26	6.8	146.1	909.3	307.2	0.306	309.2	3.26
		ε_{IHX}: 50%	132.5	945.8	7.14	6	167	942	299.5	0.219	333.6	3.34
		% Variation				−13.33	12.51	3.47	−2.57	−39.73	7.31	2.40
R290	T_k: 40 °C	ε_{IHX}: 0%	137.2	1369.4	9.98	4.4	227.3	728.3	478.4	0.456	326.3	2.09
		ε_{IHX}: 50%	137.2	1369.4	9.98	3.5	287.7	776.7	449.1	0.312	363.8	2.23
		% Variation				−25.71	20.99	6.23	−6.52	−46.15	10.31	6.28
	T_k: 20 °C	ε_{IHX}: 0%	137.2	836.5	6.10	3.5	282.8	906.2	298	0.323	304.9	3.36
		ε_{IHX}: 50%	137.2	836.5	6.10	3.1	326	919.6	293.4	0.22	332.9	3.41
		% Variation				−12.90	13.25	1.46	−1.57	−46.82	8.41	1.47
R1270	T_k: 40 °C	ε_{IHX}: 0%	173.8	1648.4	9.48	4.2	237.5	926.2	474.4	0.44	335.2	2.11
		ε_{IHX}: 50%	173.8	1648.4	9.48	3.4	293.8	963.9	455.6	0.308	373.7	2.19
		% Variation				−23.53	19.16	3.91	−4.13	−42.86	10.30	3.65
	T_k: 20 °C	ε_{IHX}: 0%	173.8	1017.0	5.85	3.4	292	1138.7	297.5	0.312	311.7	3.36
		ε_{IHX}: 50%	173.8	1017.0	5.85	3	332.5	1139.4	296.9	0.217	340.2	3.37
		% Variation				−13.33	12.18	0.06	−0.20	−43.78	8.38	0.30

3.1. Experimental set-up description

The experimental plant used for the evaluation of the refrigerant mixtures is schematized in Fig. 2. The main components are: semi hermetic compressor (1), oil separator (2), brazed-plate condenser (3), liquid receiver (4), internal heat exchanger (IHX) (8), electronic expansion valve working as a thermostatic one (5), and finally, a finned-tube evaporator (6) installed inside a glass-door horizontal island for frozen food (7). Table 3 shows a detailed description of those components (dimensions, model, manufacturer…)

Both compressor heads have been externally cooled placing a fan over them, following the compressor manufacturer recommendation and due to operating conditions. The electrical consumption of this fan is constant and equal in all tests and has been included in the energy analysis.

To control the external conditions, the freezing island is placed into a climatic chamber of 3 (L) x 3.5 (H) x 3 (W) m (31.5 m^3). This climatic chamber maintains Class III environmental conditions (25 °C dry-bulb temperature; 60% RH) according to ISO 23,953–2:2015.

To maintain the desired heat sink conditions at the condenser, an external system is used as a heat sink. This external system controls the water inlet temperature and the volumetric flow rate by means of electrical resistors and a refrigeration facility. The power consumption of the pump that drives the water to the condenser has not been considered in the energy analysis.

3.2. Measurement system and uncertainties

The refrigerating facility schematized in Fig. 2 is completely instrumented with different transducers as temperature and pressure probes, two flow meters, two watt-meters and one hygrometer. The aim of these transducers is to determine the thermodynamic states of the tested fluids and to calculate the heat transfer rate in the condenser or evaporator. Table 4 summarizes the calibration range and the accuracy of these measurement devices.

Both compressors share the same suction and discharge pressure sensors.

The data acquisition system consists of two modules CRio-9025 from National Instruments® with a time sampling period of 5 s, linked to a graphical interface programmed with LabView®. Thermophysical properties of the refrigerant and the secondary fluids are calculated with RefProp® v.10.0 and the software SecCool® v.1.

Table 3
Characteristics of the main components.

Number	Component	Location	Main characteristics
1	Compressor	Machinery room	Semi hermetic compressor Used with anthropogenic refrigerants BITZER Model: 2HES-1Y-40S Displacement: 6.5 $m^3 \bullet h^{-1}$ (1450 rpm) Used with Hydrocarbon refrigerants DORIN Model HEX181CC Displacement: 7.5 $m^3 \bullet h^{-1}$ (1450 rpm) Lubricant oil used in all cases: POE SL32
2	Oil separator	Machinery room	Hermetic oil separator Used with anthropogenic refrigerants ESK Model: OS-12. Volume: 2.3 dm^3 Used with Hydrocarbon refrigerants ESK Model: OS-12. Volume: 2.3 dm^3
3	Condenser	Machinery room	Insulated brazed plate heat exchanger SWEP Model: B25-THX40 (40 plates) Heat transfer area: 2.39 m^2 Secondary fluid: water
4	Liquid receiver	Machinery room	Insulated liquid receiver TECNAC Volume: 5 dm^3
5	Expansion valve	Climatic chamber	Electronic expansion valve CAREL E2V11
6	Evaporator	Climatic chamber	Finned-tube heat exchanger from SEREVA. Tube of 3/8'' staggered array with fine spacing if 8 mm Heat transfer area (internal tube): 1.35 m^2
7	Freezing island	Climatic chamber	Horizontal island from FROST-TROL with glass doors. Dimensions: 1875 (L) x 1170 (H) x 1000 (W) mm Defrosting with electrical resistors: 2600 W
8	IHX	Climatic chamber	Inner tube heat exchanger PACKLESS Model: HXR-50 Heat transfer area (internal tube): 0.022 m^2
9	Product	Climatic chamber	M-test package (ISO-15,502). Dimensions: 200 x 100 x 50 mm

3.3. Test methodology

An electronic expansion valve working in thermostatic mode, controls the evaporation at the freezing cabinet. For a proper operation of

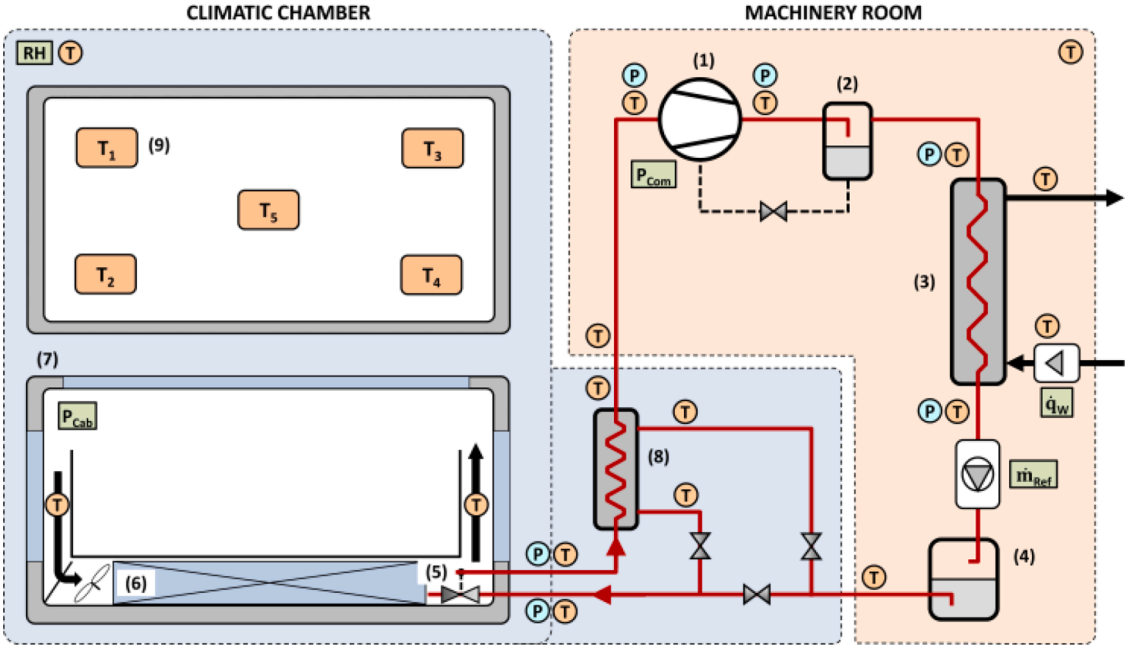

Fig. 2. Schematic layout of the refrigeration system and measurement devices.

Table 4
Characteristics and accuracy of the measurement elements.

Number	Variable	Type	Calibration range	Accuracy
21	Temperature	T-type thermocouple	−40 to 125 °C	± 0.5 °C
4	Pressure	Pressure gage JOHNSON CONTROLS P499	0 to 30 bar	± 0.08 bar
3	Pressure	Pressure gage JOHNSON CONTROLS P499	0 to 16 bar	± 0.04 bar
1	Mass flow rate	Coriolis flow meter YOKOGAWA ROTAMASS RCCT34	0 to 0.1 kg•s^{-1}	± 0.1% lecture
1	Volumetric flow rate	Magnetic flow meter YOKOGAWA RXF032G	0 to 2.5 m^3•h^{-1}	± 0.25% lecture
1	Electric Power	Single phase digital Wattmeter SENECA Z203	0 to 3000 W	± 0.5% lecture
1	Electric Power	Three phases digital Wattmeter GOSSEN METRAWATT A210	0 to 2500 W	± 0.5% lecture
1	Dry-bulb temperature	Humidity and temperature transducer CAREL DPPC	−20 to 80 °C	± 0.5 °C
	Relative humidity		5 to 98%	± 5%

the experimental facility, avoiding instabilities, the superheating at the evaporator outlet is set to 15 K. The saturation curve of each refrigerant is programmed at the expansion valve control module, using data from RefProp® v10.0.

The defrosting period of 8 h programmed by the cabinet manufacturer is adopted in this work, regardless the refrigerant tested. As defrosting method is used the additional heat supplied with electrical resistors is used until they are switch off when the temperature sensor placed over the finned surface reaches 5°C.

The freezing cabinet is located at a climatic chamber where the inner conditions simulate the internal environment of the supermarket, corresponding to Class III according to ISO 23,953–2:2015 (T: 298 K ± 0.2 K and RH: 60% ±2.5%). This methodology guarantees that the same thermal loads are acting whichever the refrigerant used.

The freezing cabinet controller stops and closes the expansion valve when the air at the evaporator inlet reaches the selected value. This value (around −21°C / −22°C) is selected to keep the product at an average temperature of −20°C. At the same time, the product average temperature is monitored using five thermocouples inserted in five packages distributed along and wide the freezing cabinet (see Fig. 2)

The compressor running frequency was kept at 1500 rpm in all cycle conditions and tests. The governance strategy adopted to stop the compressor is an on/off regulation by means of a pressure switch installed at the compressor suction port. The pressure switch is adjusted to provide a low-cut temperature of −50 °C (0.81 bar for R404A; 0.58 bar for R468A, 0.59 bar for R455A, 0.55 bar for R454C, 0.91 bar for R290 and 0.70 bar for R1270). This regulation mode is somewhat outdated, if we compare it with a frequency regulation mode for instance but assures that all the refrigerants are tested at similar cycle and compressor conditions.

The test began when the products reach the reference temperature value of −20°C in average. The tests last for 16 h of continuous running including two defrosting cycles. Throughout this period were kept constant the heat sink temperature and the water mass flow rate for each outdoor conditions tested (20°C, 30°C and 40°C). This methodology allows to consider the heat transfer at the condenser.

The sampling period was 5 s, which meant 17,280 samples per sensor and test. Table 5 summarize the averaged test conditions without IHX and with IHX at each condensing level. The standard deviation of each parameter is calculated and shown beside the corresponding mean value. It demonstrates the high stability of the measured parameters.

Two main conclusions arise from the data gathered at those tables. First, all test conditions are kept quite constant during the test duration. Second, all refrigerants are capable of cooling and conserve the product

Table 5
Test conditions summary with and without IHX (averaged along 16 h).

	With and without IHX						
		Heat sink temperature					
Refrigerant	**Parameter**	**20**		**30**		**40**	
		No IHX	**IHX**	**No IHX**	**IHX**	**No IHX**	**IHX**
R404A	Heat sink temperature (°C)	20.16±0.4	20.08±0.31	29.54±0.57	30.02±0.71	39.83±0.31	39.84±0.34
	Heat sink flow rate (m^3•h^{-1})	0.40± 0.0009	0.40± 0.0009	0.40± 0.0009	0.40± 0.0009	0.40± 0.0009	0.40± 0.0011
	Climatic chamber temperature (°C)	25.43±0.20	25.46±0.19	25.46±0.17	25.43±0.17	25.43±0.20	25.56±0.11
	Climatic chamber relative humidity (%)	58.75±2.14	58.65±2.07	59.01±1.92	58.85±1.72	58.88±2.02	59.12±1.57
	Average product temperature (°C)	−19.99± 0.35	−20.22± 0.3	−20.41± 0.47	−20.07± 0.31	−19.94± 0.42	−19.94± 0.33
R468A	Heat sink temperature (°C)	20.31±0.36	20.30±0.36	29.99±0.24	20.18±0.20	39.75±0.14	39.66±0.00
	Heat sink flow rate (m^3•h^{-1})	0.40± 0.0010	0.40± 0.0009	0.40± 0.0009	0.40± 0.0012	0.40± 0.0010	0.40± 0.0009
	Climatic chamber temperature (°C)	25.45±0.22	25.44±0.21	25.40±0.21	25.58±0.10	25.41±0.23	25.46±0.21
	Climatic chamber relative humidity (%)	58.61±2.47	58.48±2.57	58.63±2.51	59.08±1.44	58.41±2.58	58.52±2.47
	Average product temperature (°C)	−19.98± 0.04	−20.58± 0.33	−20.20± 0.49	−20.49± 0.30	−20.00± 0.60	−19.88± 0.40
R455A	Heat sink temperature (°C)	20.14±0.16	20.21±0.25	30.07±0.18	30.12±0.19	39.64±0.23	39.95±0.19
	Heat sink flow rate (m^3•h^{-1})	0.40± 0.0008	0.40± 0.0010	0.40± 0.0011	0.40± 0.0010	0.40± 0.0009	0.40± 0.0012
	Climatic chamber temperature (°C)	24.99±0.26	25.00±0.27	25.22±0.26	25.04±0.27	25.26±0.20	25.30±0.26
	Climatic chamber relative humidity (%)	58.53±2.89	58.46±2.86	58.43±2.71	58.56±2.88	57.97±2.70	58.66±2.75
	Average product temperature (°C)	−19.54± 0.39	−20.14± 0.40	−19.60± 0.39	−20.00± 0.41	−19.60± 0.39	−20.00± 0.45
R454C	Heat sink temperature (°C)	20.29±0.23	20.41±0.36	30.15±0.21	29.94±0.18	40.10±0.35	39.99±0.27
	Heat sink flow rate (m^3•h^{-1})	0.40± 0.0010	0.40± 0.0009	0.40± 0.0012	0.40± 0.0008	0.40± 0.0012	0.40± 0.0010
	Climatic chamber temperature (°C)	25.42±0.23	25.45±0.22	25.44±0.19	25.38±0.27	25.45±0.22	25.40±0.22
	Climatic chamber relative humidity (%)	58.73±2.49	58.64±2.48	58.86±2.12	60.50±2.32	58.71±2.48	58.50±2.62
	Average product temperature (°C)	−19.73± 0.5	−19.94± 0.27	−19.91± 0.43	−20.21± 0.52	−20.00± 0.56	−19.99± 0.32
R290	Heat sink temperature (°C)	20.08±0.19	19.96±0.19	29.81±0.13	29.88±0.13	39.90±0.24	39.87±0.15
	Heat sink flow rate (m^3•h^{-1})	0.40± 0.0009	0.41± 0.0009	0.40± 0.0011	0.40± 0.0010	0.40± 0.0009	0.40± 0.0011
	Climatic chamber temperature (°C)	25.40±0.13	25.38±0.22	25.49±0.14	25.31±0.23	25.25±0.27	25.30±0.19
	Climatic chamber relative humidity (%)	58.89±1.27	57.32±3.18	58.45±1.87	58.26±2.74	58.63±2.40	58.46±2.35
	Average product temperature (°C)	−19.93± 0.36	−20.06± 0.34	−19.95± 0.38	−19.97± 0.38	−19.84± 0.42	−20.00± 0.45
R1270	Heat sink temperature (°C)	20.09±0.26	20.02±0.25	29.67±0.21	30.14±0.65	39.79±0.32	39.70±0.24
	Heat sink flow rate (m^3•h^{-1})	0.40± 0.0011	0.40± 0.0010	0.40± 0.0011	0.40± 0.0009	0.40± 0.0010	0.40± 0.0009
	Climatic chamber temperature (°C)	25.47±0.22	25.33±0.22	25.24±0.25	25.19±0.23	25.19±0.26	25.22±0.23
	Climatic chamber relative humidity (%)	57.14±3.03	57.35±3.03	57.47±3.05	57.52±3.02	57.42±3.10	57.39±3.11
	Average product temperature (°C)	−20.00± 0.41	−20.33± 0.31	−20.19± 0.33	−20.33± 0.35	−20.11± 0.37	−20.00± 0.47

at the desired frozen temperature.

According with JCGM (Joint Committee for Guides in Metrology (JCGM) 2008),0 the uncertainty of directly measured parameters (u_D), being those pressure, temperature, relative humidity, electrical consumption volumetric and mass flow rates, has been estimated taking into account the standard deviation (u_σ), and the accuracy of the measurement (u_M) devices. The first one is obtained from measured data, and the second one, from that provided by device manufacturers. It has been supposed a gaussian distribution for the uncertainties with a 95% level of confidence, so the expression used to calculate u_D is that proposed in Coleman (Coleman and Steele 2009), shown in Eq.9.

$$u_D = t_{95}\cdot\sqrt{u_M{}^2 + u_\sigma{}^2} \approx 2\cdot\sqrt{u_M{}^2 + u_\sigma{}^2} \tag{9}$$

Being t_{95} the distribution factor of the uncertainty with a 95% level of confidence, which is approximated to 2.

Uncertainty related to thermodynamic properties (u_{TH}), like enthalpy or specific volume, is calculated using the methodology explained by Moffat (Moffat, 1985). Eqs. (10) to 13 synthetize this methodology.

$$prop_{TH} = f(x,y) \tag{10}$$

$$u_{TH,x} = \frac{prop_{TH}(x - u_{D,x}, y) + prop_{TH}(x + u_{D,x}, y)}{2} \tag{11}$$

$$u_{TH,y} = \frac{prop_{TH}(x, y - u_{D,y}) + prop_{TH}(x, y + u_{D,y})}{2} \tag{12}$$

$$u_{TH} = \sqrt{u_{TH,x}^2 + u_{TH,y}^2} \tag{13}$$

Where:

- $prop_{TH}$ is the thermal property, function of the directly measured parameters x, and y
- $u_{TH,x}$ is the partial uncertainty of the thermal property as function of the parameter x
- u_{THy} is the partial uncertainty of the thermal property as function of the parameter y
- u_{TH} is the uncertainty related to the thermal property

The uncertainties of indirect parameters ((ε_I), like cooling capacity and IHX effectiveness, takes into account the error propagation from directly measured parameters. They are evaluated using the Taylor series expansion for error propagation, with a 95% level of confidence, too. The expression used is shown in Eq. (14).

$$\varepsilon_I = t_{95}\cdot\sqrt{\sum_i^N \left(\left(\frac{\partial F}{\partial X_i}\right)^2 \cdot \varepsilon_i^2\right)} \tag{14}$$

Where:

-F is the function to calculate the indirect parameter

- ε_i is the uncertainty related to the directly measured parameters or the thermodynamic properties

- X_i are the variables used in function F

-N is the number of variables of the function F

4. Analysis of experimental results

In this section, the variations produced on the main parameters affected by the connection of an IHX are shown. For purposes of clarity, these variations are presented in absolute or relative values. The relative variations are calculated as a percentage regarding values without IHX.

As the refrigeration facility is under a dynamic regime, due to the continuously thermostatic valve regulation and compressor start and stop throughout the 16 h test, the parameters of the associated vapor compression cycle are continuously in transitional regime. That the reason is why these parameters are averaged during the time the compressor is “on”, and when the compressor electrical consumption is between a maximum and a minimum value, see Fig. 3.

4.1. Cycle parameters

In Fig. 4 are shown the phase change temperatures as well as the compression ratio variations when the IHX is activated. The evaporating temperature is evaluated using Eq.15, while condensing temperature is calculated with Eq.(16). Both expressions are derived from ASERCOM criteria (ASERCOM 2015), and RefProp® v.10.0 is used for calculation.

$$T_o = \frac{T_{o,in}(h_{in}, p_{o,in}) + T_{v,sat}(p_{o,out})}{2} \tag{15}$$

$$T_k = \frac{T_{liq,sat}(p_{k,in}) + T_{k,sat}(p_{k,out})}{2} \tag{16}$$

Compression ratio is equal to the ratio between discharge and suction pressures.

In case condensing temperatures the variations are negligible, except R468A at 30°C heat sink temperature test, but the relative variation in this case is lower that 10%. Evaporating temperatures experience a slight decrease not further than 1 °C in all operating conditions and refrigerants tested. This reduction in evaporating pressure, is enhanced with the additional pressure drops at the suction line produced by the IHX, resulting in an increase in the compression ratio, not higher than 3%. Additional pressure drops in suction line are 4.5% on average, although it depends strongly on the mass flow rate variation and on the refrigerant tested. So, in view of data shown in Fig.4, it could be concluded that these three parameters are not significantly affected when the IHX is activated.

The effects on main cycle parameters related to the additional superheat generated by the IHX on the suction line are shown in Fig. 5. In this case, the compressor suction temperature is the parameter directly affected. It shows 9.7 K, 11.6 K and 12.9 K of mean increases at 293 K, 303 K and 313 K heat sink temperature tests. So, IHX makes greater increases in temperature at compressor inlet as the heat rejection temperature increases. Regarding the specific volume at the compressor suction port, it undergoes an increment from 4.61 K on average at 293 heat sink temperature tests, to 6 K on average at 313. From the short difference between increases it can be stated that there is no great dependence on the heat sink temperature. This increment is partially because of the additional pressure drop introduced by the IHX, but, mainly, because of the compressor suction temperature rise, which is common to all tests done, with 11.4 K on average. However, this increase is not reflected in a similar increase in the discharge temperature. Practically disappears and compressor discharge temperature seems not to be affected, even it decreases in some tests. This attenuation is consequence of the significant compressor running time reduction when the IHX is activated, what allows a greater cooling time of the compressor discharge port (see Fig. 8).

Fig. 6 shows the effects on main cycle parameters related to the additional subcooling produced at the liquid line when the IHX is connected. In first term, the reduction in the inlet temperature at the expansion valve is shown. This parameter is reduced 9.6 K, 12.6 K and 13.9 K on average at 293 K, 303 K and 313 K heat sink temperatures respectively, so the reduction is greater as greater the heat sink temperature is. This effect is translated into a 20% reduction on average in the vapor quality at evaporator inlet. The reduction in the vapor quality at evaporator could be the responsible of the decrease in the evaporating pressure shown Fig. 4, since this fact cause a greater average density at evaporator when the IHX is operating. The specific cooling capacity is directly affected by the reduction in the expansion valve temperature inlet and the vapor quality. This parameter shows a clear increment of 8.8%, 12.4% and 15.9% on average with 292 K, 303 K and 313 K heat sink temperature tests, respectively. That is, great augmentation in q_o as

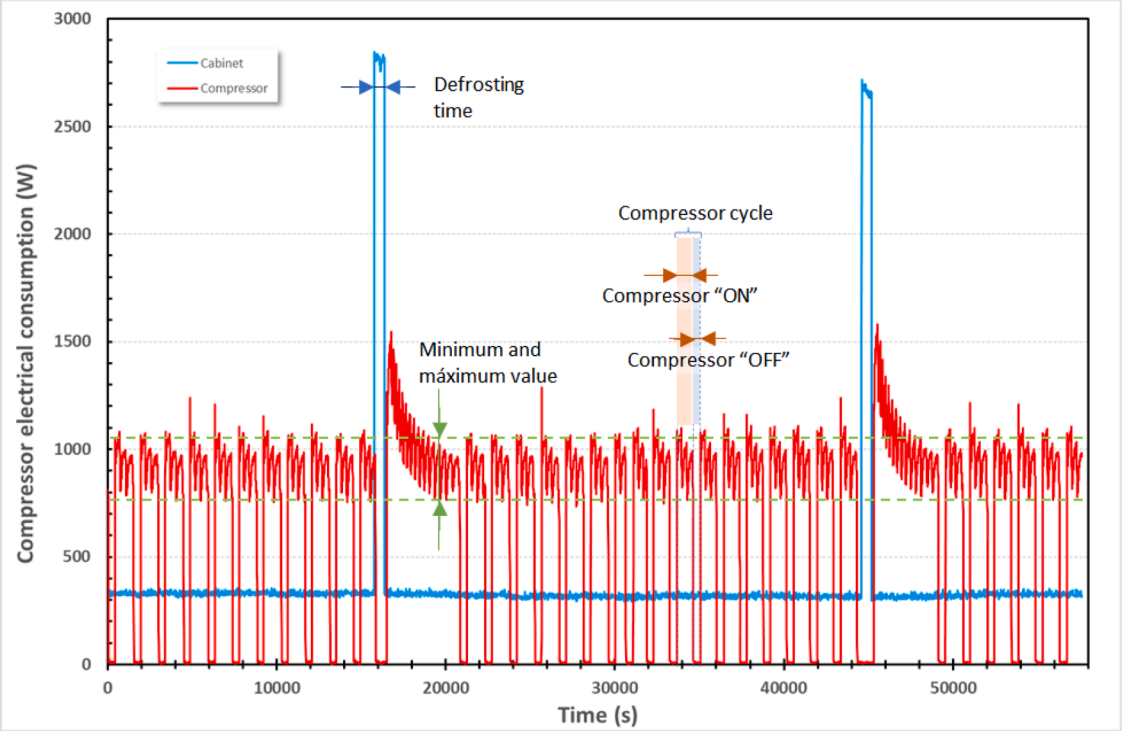

Fig. 3. Compressor electrical power consumption during a 16 h test.

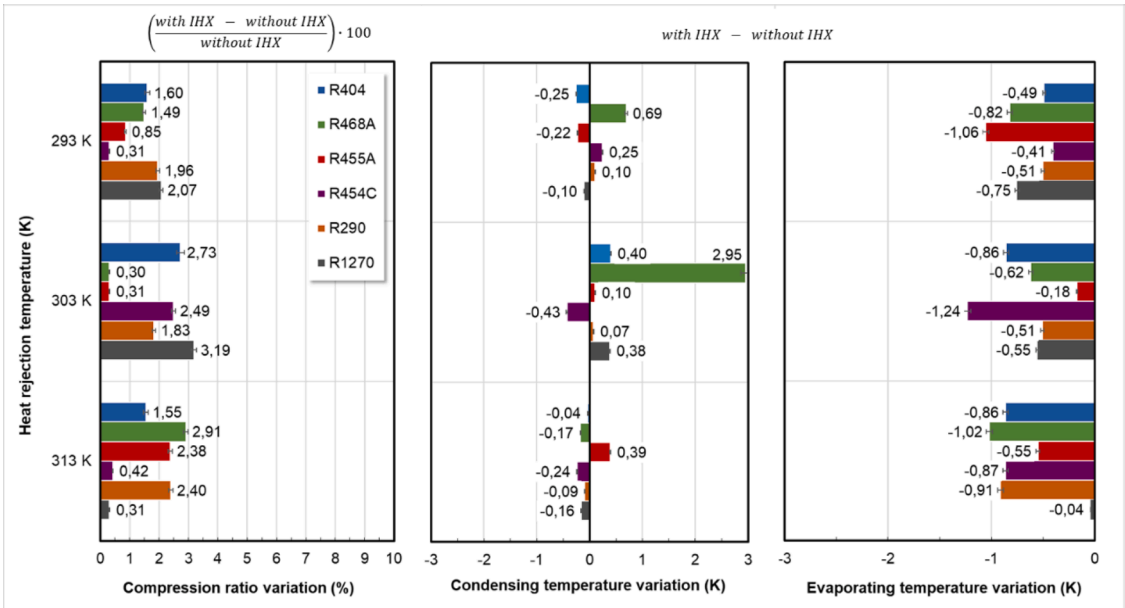

Fig. 4. Variations in phase change temperatures and compression ratio.

hotter the heat sink temperature is.

The volumetric cooling capacity (VCC) and COP are the two last cycle parameter variations commented at this section. They are calculated using Eqs. (6) and (7), where the enthalpies are average values, as is explained at the beginning of this section and the value obtained are depicted at Fig. 7. Such VCC~~e~~ like COP present increases when IHX is activated. Thus, VCC is augmented 4.0%, 7.0% and 9.3% on average, while COP is augmented 19.6%, 27.5% and 31.2% on average at 293 K, 303 K and 313 K heat sink temperature tests, respectively~~, in both cases~~. Increments of both parameters are higher as higher is the heat rejection temperature. Variation in VCC is smoother than the COP one, due to the increment in q_o is counterbalanced with the increment in compressor suction specific volume, while in the case of COP, the increment in q_o is boosted with the reduction of the specific compression work, making a great rise in COP when IHX is activated.

The reduction in compression specific work when IHX is operating is not real if were analyzing the thermodynamic cycle, because the time reduction in which the compressor is ON, produces a minor heating in the discharge port, so the mean discharge temperature measured is minor than that measured when IHX is not operating. This is an effect of the dynamic behavior of the refrigerating facility that has to be taken into account and allows only qualitative interpretations but not

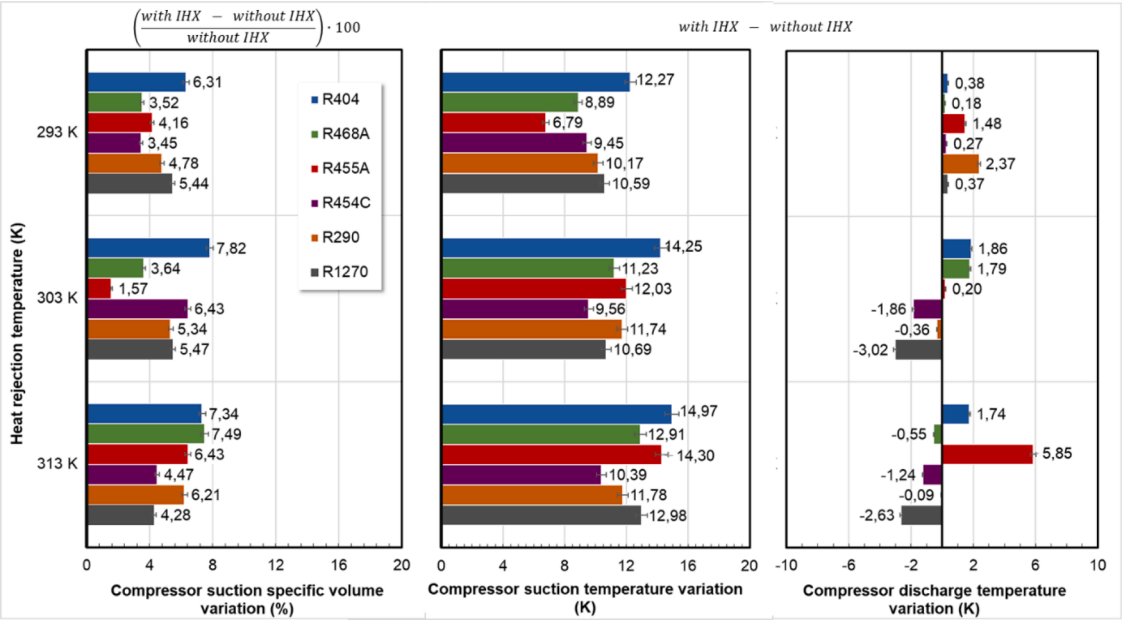

Fig. 5. Variations in compressor suction temperature and specific volume, as well as in compressor discharge temperature.

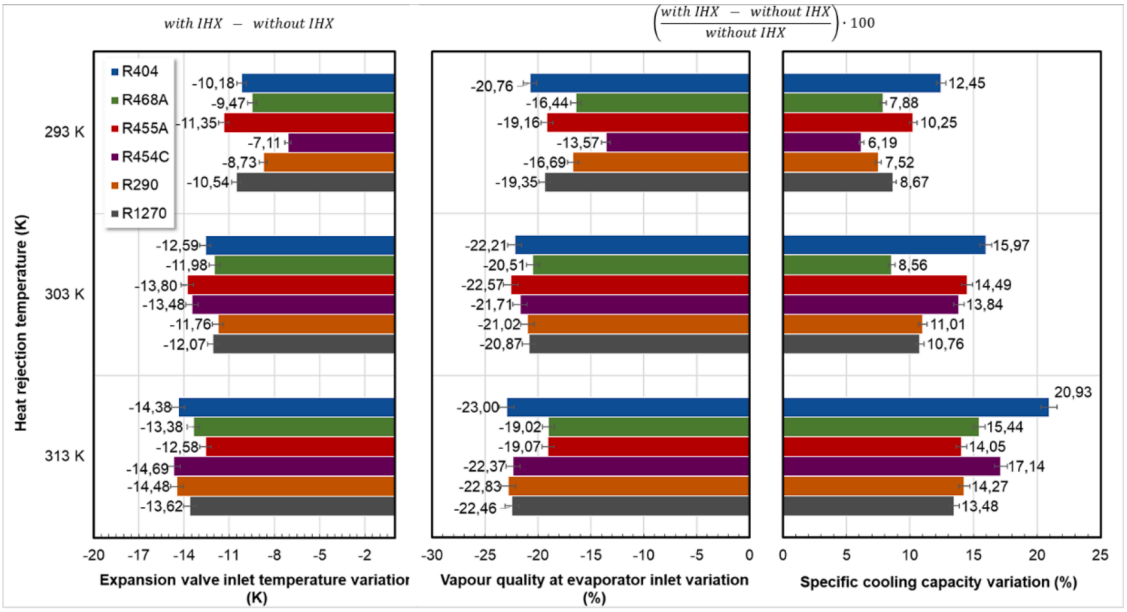

Fig. 6. Variations in expansion inlet temperature, vapor quality at evaporator inlet and specific cooling capacity.

quantitative ones.

4.2. Energy consumption parameters

At this section the variation in the energy performance of the vapor compression cycle once the IHX is operating is analyzed.

Considering the compressor cycle as the time between two consecutively compressor starts (see Fig.3), Table 6 gathers the number of compressor cycles and the time the compressor is ON during the whole test, obtained at 30°C heat sink temperature tests. The other heat sink temperatures present the same behavior and do not add valuable information, so it does not appear in this paper in order to shorten its length.

It is observed that number of refrigeration cycles increase when IHX activated. R404A and R290 are the refrigerants with a greater increase, while R455A is the one with lower increase. This increase in compressor cycling frequency is due to the increase in cooling capacity, and also affects the compressor working time. As major cooling capacity, minor is the time needed to abate the internal air temperature, considering that the cooling duty or the thermal loads are the same.

In Fig. 8 in first term the IHX effectiveness obtained for each refrigerant at every heat sink temperature is shown. The value, in general, is greater as lower the heat sink temperature is with 44.4%, 36.0% and 24.8% on average at 293 K, 303 K and 313 K heat sink temperature tests, respectively. The compressor operation time is reduced regardless of the refrigerant used and the heat sink temperature. Mean reductions in compressor operating time are 5.8%, 6.0% and 9.7% at average at 293 K, 303 K and 313 K heat sink temperature tests, respectively. It

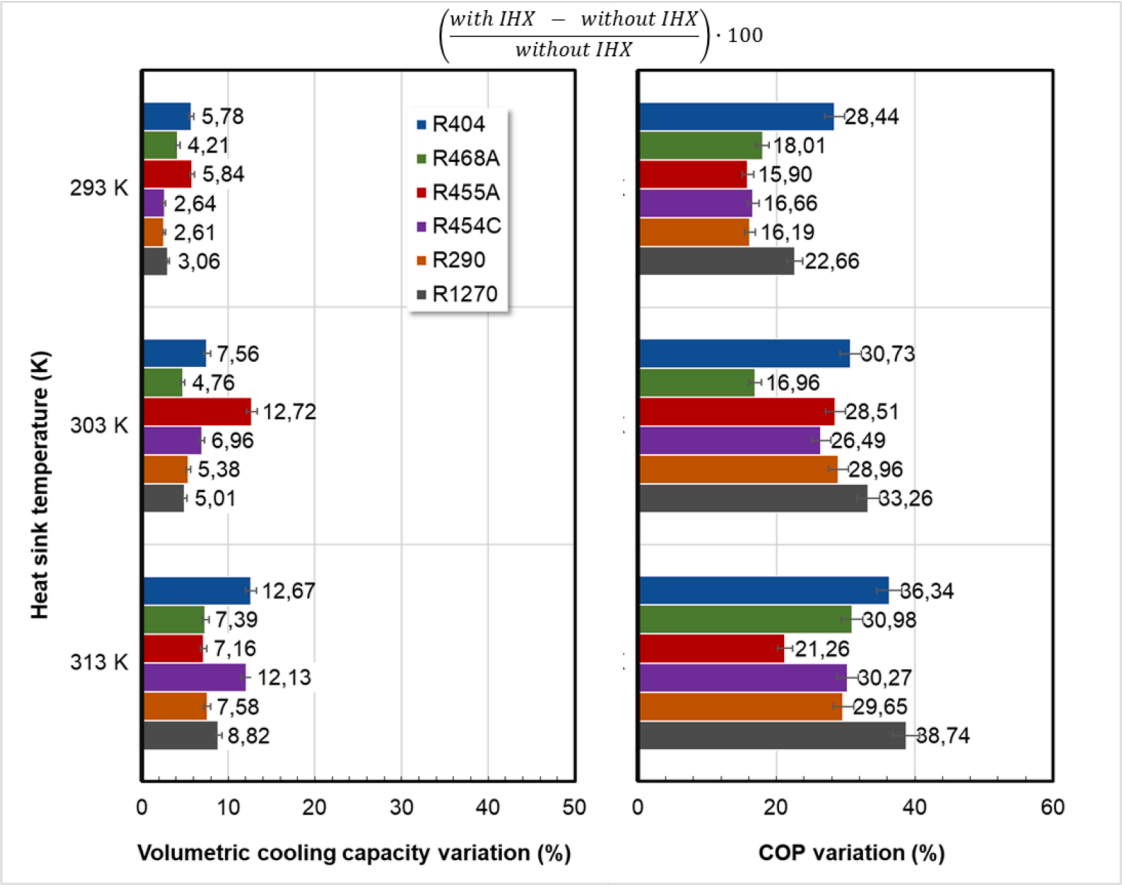

Fig. 7. Variations cycle volumetric cooling capacity, evaporator cooling capacity and COP.

Table 6
Number of compressor cycles and time compressor is ON, in 30°C tests.

	R404A		R468A		R454C		R455A		R290		R1270	
30 °C	**IHX**	**No IHX**	**IHX**	**No IHX**	**IHX**	**No IHX**	**IHX**	**No IHX**	**IHX**	**No IHX**	**IHX**	**No IHX**
Number of cycles	50	36	39	30	50	43	43	39	48	37	59	51
Compressor ON (min)	628.7	709.4	753.5	797.9	682.9	716.2	647.6	738.4	668.1	713.8	587.6	635.9

shows an inverse trend to that shown by the IHX effectiveness, which is reduced in major term as greater this temperature is. It seems not to exist any direct correlation between IHX thermal effectiveness and compressor operation time trends.

Finally, the total energy consumption of the facility during the 16-hour tests is shown. This parameter has been calculated from the electrical consumption measurements and operating time of each element using a trapezoid integration method. The resulting equation is shown in Eq. (17), where 'i' represents each energy consuming device (compressor, cooling cylinder head fan and freezing island), 'P_C' its corresponding power consumption and 'j' each sampled data. The difference between two samples is five seconds and the expression is evaluated during the 24-hour test.

$$E_i = \frac{1}{36\cdot 10^5}\cdot \int_0^{24h} P_{C,i}(t)\cdot dt = \sum_{j=1}^{24h}\left[\frac{P_{C,i}(j)+P_{C,i}(j-1)}{2}\right]\cdot[t(j)-t(j-1)] \quad (17)$$

The compressor is the only component that presents different consumption values depending on the operating conditions and the refrigerant used as working fluid. The differences obtained at the total energy consumption are derived from the variation of the energy consumption in the compressor.

It is observed that the total energy consumption is reduced in all the operation conditions when the IHX is activated. This reduction is, higher as higher the heat sink temperature is. So, mean reduction are 0.8 kWh, 0.92 kWh and 1.51 kWh each 16 h, at 293 K, 303 K and 313 K heat sink temperature tests, respectively. This higher reduction in electrical energy consumption as hotter the rejection temperature is, is mainly because the higher q_o obtained in the same conditions (see Fig.6), since this allows major cooling capacity and in consequence minor compressor operating time.

The total energy reduction increases with the heat sink temperature increase, so this fact allows as to say that IHX improves the energy performance of the freezing cabinet yielding in better improvements as worst the sink temperature is.

5. Conclusions

At this work, the energy performance of a freezing cabinet with and without an IHX activated has been compared. The comparison has been carried out using the R404A as the standard refrigerant used nowadays, and five low-GWP alternative refrigerants: R468A, R455A, R454C, R290 and R1270. Besides, it is based on experimental data obtained in a real freezing facility working in a wide range of heat sink temperatures (20°C, 30°C and 40°C).

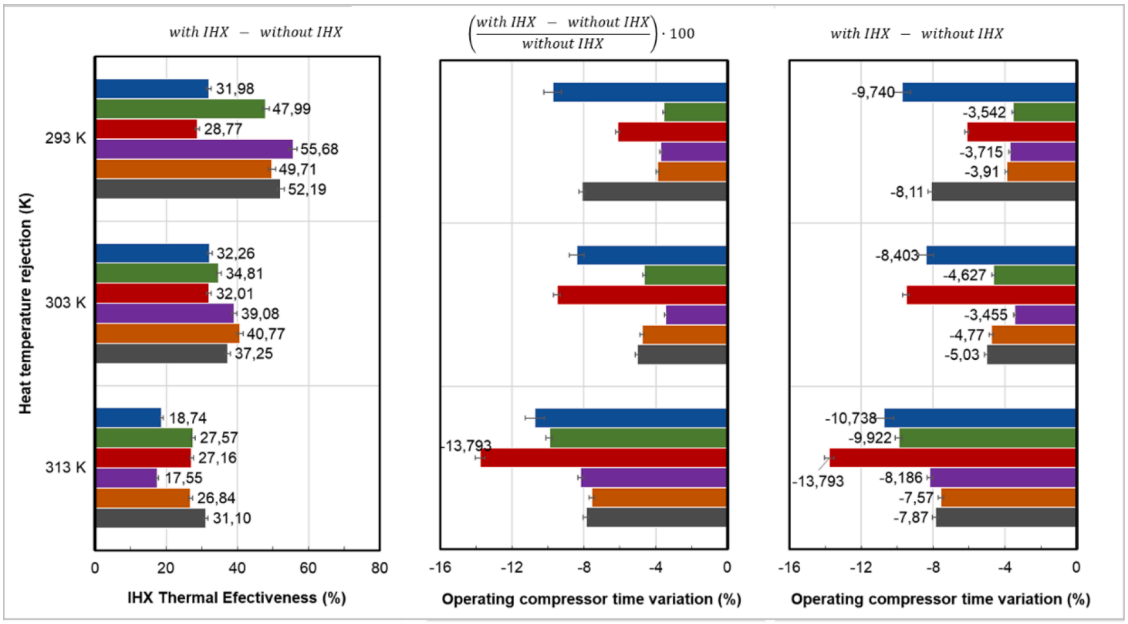

Fig. 8. IHX effectiveness and variations in operating compressor time and total energy consumption.

The placement of an IHX does not disturb the proper operation of the freezing cabinet, being able to achieve the internal set temperature (−20°C) with all the refrigerants and operating conditions.

The refrigeration system increases the compressor cycling frequency with all the refrigerants, resulting in a decrease in the time the compressor is ON. This fact allows that the compressor discharge temperature suffers a very slight increment, much lower than the increase in compressor suction temperature. In any case, the discharge compressor temperature increases above a dangerous value not recommended by lubricant manufacturers.

The introduction of an IHX placed at the freezing island allows a reduction that ranges from 7.12% to 8.49% of the total energy consumed in the case of using R404A, from 3.01% to 7.79% in case of using R468A, from 4.90% to 9.60% in case of using R455A, from 3.25% to 6.95% in case of using R454C, from 2.98% to 6.01% in case of using R290 and from 8.06% to 8.45% in case of using R1270.

The reduction in energy consumption generated by the IHX is greater when greater the heat sink temperature is in all cases.

Thermodynamic analysis done in Section 2 agree qualitatively with experimental data, since both show the energy improve produced by the IHX, and its greater benefic effect as greater is the heat sink temperature, but not agree in the actual values.

From this study, we extract the main conclusion that freezing cabinets (remote or self-contained) should be equipped with an IHX, regardless the refrigerant used, because it will suppose an upgrade in their energy performance with low invest.

Declaration of Competing Interest

The authors declare that they have no known competing financial interests or personal relationships that could have appeared to influence the work reported in this paper.

Acknowledgments

The authors gratefully acknowledge the Ministerio de Ciencia y Tecnología – Spain (project RTI2018–093501-B-C21) and the Jaume I University (project UJI-B2019–56) for financing this research work.

8. References

AIRAH 2012 Methods of calculating total equivalent warming impact (TEWI) 2012 AIRAH, The Australian Institute of Refrigeration, Air Conditioning and Heating (2012).

Makhnatch, P., Khodabandeh, R., 2014. The role of environmental metrics (GWP, TEWI, LCCP) in the selection of low GWP refrigerant. Energy Procedia 61. https://doi.org/10.1016/j.egypro.2014.12.023 https://doi.org/.

Lebrun, P., Ziegler, F., 2019. 38th informatory note on refrigeration technologies. The Role of Refrigeration on the Global Economy. https://doi.org/10.18462/iif.NItec38.06.2019. Junehttps://doi.org/.

Directive (EU) 2018/2002 of the European Parliament and of the Council of 11 December 2018 amending Directive 2012/27/EU on energy efficiency. http://data.europa.eu/eli/dir/2018/2002/oj.

Gosney, W.B., 1982. Principles of Refrigeration. Cambridge University Press. ISBN: 0521236711.

Emerson Climate Technologies. Compressor Overheating. Application Engineering Bulletin. AE17-1260. March 1993. https://climate.emerson.com/CPID/GRAPHICS/Types/AEB/ae1260.pdf.

Domanski, P.A., Didion, D.A., Doyle, J.P., 1994. Evaluation of suction line–liquid line heat exchange in the refrigeration cycle. Int. J. Refrig. 17 (7), 487–493.

Domanski P.A. Theoretical evaluation of the vapour compression cycle with a liquid-line/suction-line heat exchanger, economizer and ejector NISTIR 5606 1995.

Aprea, C., Ascani, M., de Rossi, F., 1999. A criterion for predicting the possible advantage of adopting a suction/liquid heat exchanger in refrigerating system. Appl. Therm. Eng. 19, 329–336.

Klein, S.A., Reindl, D.T., Brownell, K., 2000. Refrigeration system performance using liquid-suction heat exchangers. Int. J. Refrig. 23, 588–596.

Ahnefeld, G., Vollmer, D., Wobst, E, 1996. Energetic assessment of HFC-blends as R 22 alternatives. KI, Luft- und KaltetechnikVolume 32 (Issue 5), 202–208.

Boewe, D.E., Bullard, C.W., Yin, J.M., Hrnjak, P.S., 2001. Contribution of internal heat exchanger to transcritical R-744 cycle performance. HVAC R Res. 7 (2), 155–168.

Kim, M., 2002. Performance evaluation of R-22 alternative mixtures in a breadboard heat pump with pure cross-flow condenser and counter-flow evaporator. Energy 27, 167–181.

Zhang, C., Graham, B., and Dickson, T., "How to Improve Vehicle R134a A/C System Performance with a Liquid Line Suction Line Heat Exchanger (IHX)," SAE Technical Paper. 2002-01-0507, 2002, https://doi.org/10.4271/2002-01-0507.

Navarro-Esbri, J., Cabello, R., Torrella, E., 2005. Experimental evaluation of the internal heat exchanger influence on a vapour compression plant energy efficiency working with R22, R134a and R407C. Energy 30, 621–636.

Torrella, E., Sánchez, D., Llopis, R., Cabello, R. Energetic evaluation of an internal heat exchanger in a CO2 transcritical refrigeration plant using experimental data, 2022.

Sánchez, D., Patiño, J., Llopis, R., Cabello, R., Torrella, E., Fuentes, F.V., 2014. New positions for an internal heat exchanger in a CO2 supercritical refrigeration plant. Experimental analysis and energetic evaluation. Appl. Therm. Eng. 63 (1), 129–139.

Purohit, N., Gupta, D.K., Dasgupta, M.S., 2018. Experimental investigation of a CO2 trans-critical cycle with IHX for chiller application and its energetic and exergetic evaluation in warm climate. Appl. Therm. Eng. 136, 617–632.

Cao, F., Ye, Z., Wang, Y., 2020. Experimental investigation on the influence of internal heat exchanger in a transcritical CO2 heat pump water heater. Appl. Therm. Eng. 168.

Ye, Z., Wang, Y., Song, Y., Yin, X., Cao, F., 2020. Optimal discharge pressure in transcritical CO2 heat pump water heater with internal heat exchanger based on pinch point analysis. Int. J. Refrigerat. 118, 12–20.
Zhang, Z.-Y., Ma, Y.-T., Wang, H.-L., Li, M.-X., 2013. Theoretical evaluation on effect of internal heat exchanger in ejector expansion transcritical CO2 refrigeration cycle. Appl. Therm. Eng. 50 (1), 932–938.
Joneydi Shariatzadeh, O., Abolhassani, S.S., Rahmani, M., Ziaee Nejad, M., 2016. Comparison of transcritical CO2 refrigeration cycle with expander and throttling valve including/excluding internal heat exchanger: exergy and energy points of view. Appl. Therm. Eng. 93, 779–787.
Cabello, R., Sánchez, D., Llopis, R., Arauzo, I., Torrella, E., 2015. Experimental comparison between R152a and R134a working in a refrigeration facility equipped with a hermetic compressor. Int. J. Refrig. 60, 92–105.
Navarro-Esbrí, J., Molés, F., 2013. Barragán-Cervera, Á. Experimental analysis of the internal heat exchanger influence on a vapour compression system performance working with R1234yf as a drop-in replacement for R134a. Appl. Therm. Eng. 59 (1–2), 153–161.
Qi, Z., 2015. Performance improvement potentials of R1234yf mobile air conditioning system. Int. J. Refrig. 58, 35–40.
Mota-Babiloni, A., Navarro-Esbrí, J., Pascual-Miralles, V., Barragán-Cervera, Á., Maiorino, A., 2019. Experimental influence of an internal heat exchanger (IHX) using R513A and R134a in a vapor compression system. Appl. Therm. Eng. 147, 482–491.
Wantha, C., 2019. Analysis of heat transfer characteristics of tube-in-tube internal heat exchangers for HFO-1234yf and HFC-134a refrigeration systems. Appl. Therm. Eng. 157, 113747.
Cabello, R., Sánchez, D., Llopis, R., Catalán, J., Nebot-Andrés, L., Torrella, E., 2017. Energy evaluation of R152a as drop in replacement for R134a in cascade refrigeration plants. Appl. Therm. Eng. 110, 972–984.
Llopis, R., Sanz-Kock, C., Cabello, R., Sánchez, D., Torrella, E., 2015. Experimental evaluation of an internal heat exchanger in a CO2 subcritical refrigeration cycle with gas-cooler. Appl. Therm. Eng. 80, 31–41.
Llopis, R., Sanz-Kock, C., Cabello, R., Sánchez, D., Nebot-Andrés, L., Catalán-Gil, J., 2016. Effects caused by the internal heat exchanger at the low temperature cycle in a cascade refrigeration plant. Appl. Therm. Eng. 103, 1077–1086.
UNEP, 2019. 2018 Report of the Refrigeration, Air Conditioning and Heat Pumps Technical Options Committee. Ozone Secretariat, UNEP Nairobi, Kenya 300.
ASHRAE, 2019. Designation and Safety Classification of Refrigerants, Addendum y to ANSI/ASHRAE Standard 34-2019. ANSI/ASHRAE Standard 34-2019. ASHRAE.
M. G.. D. S. F. M. B. W. C. J. F. J. H. D. K. J.-F. L. D. L. B. M. T. N. A. R. G. S. T. T., Zhang, H., 2014. 2013: The Physical Science Basis. Contribution of Working Group I to the Fifth Assessment Report of the Intergovernmental Panel On Climate Change, 1st ed. London: Cambridge University Press, Cambridge, United Kingdom and New York, NY, USA.
Lemmon, M.O., Bell, E.W., Huber, I.H., McLinden, M.L., 2018. NIST Standard Reference Database 23: Reference Fluid Thermodynamic and Transport Properties-REFPROP, Version 10.0. National Institute of Standards and Technology, Gaithersburg. Standard Reference Data Program.
Woollatt, D., 1993. Factors affecting reciprocating compressor performance. Hydrocarb. Process. 72 (6).
McLinden, J.S., Domanski, M.O., Kazakov, P.A., Heo, A., Brown, J., 2012. Possibilities, limits, and tradeoffs for refrigerants in the vapor compression cycle. In: 2012 ASHRAE/NIST Refrigerants Conference.
Torrella, E., Cabello, R., Sánchez, D., Larumbe, J.A., Llopis, R., 2010. On-site study of HCFC-22 substitution for HFC non-azeotropic blends (R417A, R422D) on a water chiller of a centralized HVAC system. Energy Build. 42 (9).
Marques, P.A., Domanski, M., 1998. Potential Coefficient of Performance Improvements Due to Glide Matching with R-407C. In: International Refrigeration and Air Conditioning Conference.
M, P., MB, A., K, R., 2017. The effect of temperature glide on the performance of refrigeration systems. In: 5th IIR Conference on Thermophysical Properties and Transfer Processes of Refrigerants, p. 8.
ASERCOM, "Refrigerant Glide and Effect on Performances Declaration," no. September, pp. 1–11, 2015. https://www.asercom.org/guides/#0a0edd2b641ef8307.
Cabello, R., Sánchez, D., Llopis, R., Nebot-Andrés, L., Calleja-Anta, D., 2021. Energy evaluation of a low temperature commercial refrigeration plant working with the new low-GWP blend R468A as drop-in of R404A. Int. J. Refrig. 127, 1–11.
Joint Committee for Guides in Metrology (JCGM), "JCGM 100 2008: evaluation of measurement data - Guide to the expression of uncertainty in measurement." 2008.
Coleman and Steele, 2009. Experimentation, Validation and Uncertainty Analysis For Engineers, 3rd Edition. Wiley.
Moffat, R.J., 1985. Using uncertainty analysis in the planning of an experiment. J. Fluids Eng. 107 (2), 173-17.